



HAL
open science

Investigation of the blast pressure following laser ablation at a solid–fluid interface using shock waves dynamics in air and in water

Arsène Chemin, Mehdi Fawaz, David Amans

► To cite this version:

Arsène Chemin, Mehdi Fawaz, David Amans. Investigation of the blast pressure following laser ablation at a solid–fluid interface using shock waves dynamics in air and in water. *Applied Surface Science*, 2022, 574, pp.151592. 10.1016/j.apsusc.2021.151592 . hal-03507077

HAL Id: hal-03507077

<https://hal.science/hal-03507077>

Submitted on 5 Jan 2024

HAL is a multi-disciplinary open access archive for the deposit and dissemination of scientific research documents, whether they are published or not. The documents may come from teaching and research institutions in France or abroad, or from public or private research centers.

L'archive ouverte pluridisciplinaire **HAL**, est destinée au dépôt et à la diffusion de documents scientifiques de niveau recherche, publiés ou non, émanant des établissements d'enseignement et de recherche français ou étrangers, des laboratoires publics ou privés.



Distributed under a Creative Commons Attribution - NonCommercial 4.0 International License

Investigation of the blast pressure following laser ablation at a solid-fluid interface using shock waves dynamics in air and in water

Arsène Chemin^a, Mehdi W. Fawaz^a, David Amans^a

^a*Univ. Lyon, Université Claude Bernard Lyon 1, CNRS, UMR5306, Institut Lumière Matière, Villeurbanne, F-69100, France*

Abstract

Simple and universal relations between the laser pulse energy of the third harmonic of a Nd:YAG laser source (5 ns) and the pressure at the ablation point are investigated for the ablation of a solid target in air and in water. Shockwaves propagation are reconstructed using time-resolved shadowgraph imaging. The propagation in air is well-described by Taylor–von Neumann–Sedov’s theory for over-pressure at the shock front larger than ten times the atmospheric pressure, but the energy distribution appears to be anisotropic and mostly directed in the normal direction to the target’s surface. We compare the pressure at the shock front deduced from its velocity using Rankine-Hugoniot’s relation with the pressure deduced from Taylor’s model only related to the laser pulse energy. Rankine-Hugoniot’s relation appears more appropriate to evaluate the early pressure in the plasma plume. The shockwaves velocity in water is hyper-sonic during 50 ns and then reaches the sound velocity. Pressure values at the shock front are compared using two different approaches accounting for different state’s equations, namely the Rice and Walsh’s equation and Tait’s equation. In both cases, the ablation pressure is found out to reach several GPa and increases as the square root of the laser intensity.

Keywords: Laser Ablation in Liquids, Laser Induced Breakdown Spectroscopy, Shock waves, Shock blast, Taylor–von Neumann–Sedov, Rankine-Hugoniot, Pressure measurement

PACS: 52.38.Mf, 79.20.Ds, 52.35.Tc, 43.25.Cb, 43.28.Mw, 43.58.Dj, 47.50.Ef

Email address: david.amans@univ-lyon1.fr (David Amans)

Preprint submitted to Applied Surface Science

October 2, 2021

1. Introduction

In the framework of laser ablation based techniques, reliable and simple approaches to assess the shock pressure during laser ablation are of great interest to investigate laser ablation processes, structural modification of the target and its environment, but also laser-generated plasma thermodynamics. We show that simple approaches, well known for laser-generated shock wave in bulk fluid (air, water...), can be applied to solid/fluid interfaces in the framework of the laser source widely used for laser ablation (nanosecond and millijoule pulses). The characterisation of the shock pressure is relevant in the health field with the development of laser surgery and diagnostic on biological tissues [1, 2, 3, 4], in mechanics with laser micromachining and laser remelting [5, 6, 7], or more generally with the issue of laser-induced damages of the target [8, 9] as well as non-thermal phase transitions induced by laser [10, 11, 12]. On Mars, the SuperCam microphone records the sound from the laser-generated shock wave to determine the amount of matter removed during LIBS measurement and the softness of the target [13]. Pressure in laser-generated plasma is also a parameter of interest for LIBS [14, 15, 16] as well as for the nucleation of particles in plasmas [17]. Since the nineties [18], laser ablation in liquids is constantly proving its reliability and its versatility to produce colloidal solutions of nanoparticles [19, 20, 21, 22, 23, 24], but the characterisation of the thermodynamic conditions of temperature and pressure remains an open issue [25, 26]. The measurement of the pressure at the ablation point is no easy task. Laser-generated plasmas are transient states, with short lifetimes from a few hundreds of nanoseconds in liquids [25] to a few tens of microseconds in air [27], and usually sub-millimetric. One way to measure the pressure at the ablation spot is through the measurement of the shock wave dynamics. The shock wave dynamics in air is described by Taylor's auto-similar blast theory [28, 29] for over-pressure at the shock front larger than ten times the atmospheric pressure [30]. The model is also named the Taylor–von Neumann–Sedov's model. In the framework of laser ablation, this model is often discussed, showing its relevance despite systematic discrepancies between the shock front dynamics and the pulse energy [31, 32, 33, 34, 35, 36, 37, 38, 39, 40, 41].

The dynamics of the pressure field following a laser-induced breakdown in bulk water has been widely investigated by Vogel et al. [42]. The pressure

at the shock front can be calculated from the shock front velocity using two different analytical models: the conservation of momentum at a shock front accounting the Hugoniot’s curve data determined by Rice and Walsh [43], or the isentropic Tait’s [44] equation and Gilmore’s model. The second approach leads to lower values of the pressure [42].

In this paper, we study the dynamics of the shock waves generated by nanosecond laser pulses focused on gold, corundum aluminium oxide (alumina) and paraffin targets for a large range of pulse energy. In air, we investigate the ability of Taylor’s model to describe the shock front dynamics and the effect of the blast anisotropy on the evaluation of the pulse energy. The pressure evolution given by Taylor’s model is compared to pressure values determined from the shock front velocity using Rankine-Hugoniot’s relation. In water, the initial pressure is determined from the shock wave velocity and compared with the analytical model developed by Fabbro et al. [45] for the pressure induced by the formation of a laser-generated confined plasma.

2. Measurement Set-up

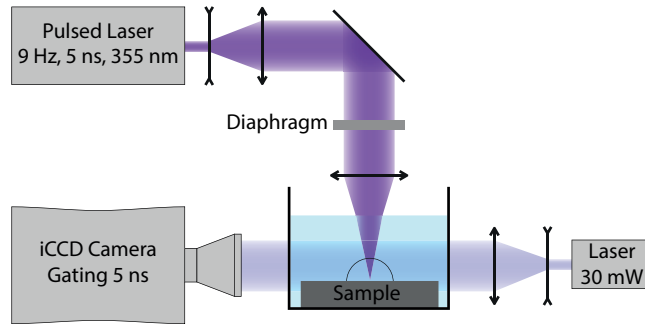


Figure 1: Outline of the measurement apparatus. For the measurements in air, the water tank is removed.

The third harmonic of a YAG-Nd pulsed laser, a Surelite laser from Continuum (355 nm, 5 ns, jitter ± 1 ns, 9 Hz, 60 mJ per pulse) is focused either on a mono-crystal of alumina, on a pure target of gold (99.99% from Neyco), or on paraffin from Roti-Plast to study metals, dielectrics and soft materials close to organics. Corundum alumina was grown by Czochralski (Cz) technique in our facilities [46, 47]. The ablation is performed at ambient

conditions either in air or for targets immersed in 1 cm of deionized water. The laser-induced hemispheric shock wave is observed using a shadowgraph imaging setup (see figure 1). The light source for the imaging is a 30 mW cw diode laser (445 nm). The gating of the intensified CCD camera from Andor (iStar 334T, 1024×1024 pixels, $13 \mu\text{m}$ size) is set to 5 ns. In literature, picosecond time resolution are achieved using an ultra-short pulsed illumination source instead of a continuous laser [48, 49], but 5 ns time resolution appears short enough to observe the shock front position and measure its velocity in a time range in which Taylor’s model is valid (large overpressure). The delay between the ablation pulse and the camera is controlled by a digital delay/pulse generator DG645 from Stanford Research Systems. The time 0 is set by the image showing the native plasma plume, 2.5 ns shifted to account for the 5 ns integration time of each image. The resolve limit of the objective (Zoom 6000 from Navitar) is $4.7 \mu\text{m}$. The resolve limit of the imaging system (iCCD and objective assembly) is $5.3 \mu\text{m}$. The spatial uncertainties are not limited by spatial resolution. The uncertainty on the shock front position at a given delay is mainly determined by the repeatability issue from pulse to pulse. For each delay, the positions of the shock front displayed in figure 2 and figure 3 correspond to the average values deduced from several repetitions of the measurement (three to five). The error bars on the shock front positions correspond to the 90% two-sided confidence interval according to the student’s t distribution and thus account for the number of measurement used to compute each average position. The pulse energies are measured with a thermal power sensor from Thorlabs, namely the S470C head connected to the PM100D console.

Figure 2 (a) shows selected images of the shock wave propagating in air and following the ablation of a gold target with a pulse energy of $3.1 \pm 0.1 \text{ mJ}$. A narrow band-pass filter (5 nm) centred on the continuous laser wavelength at 450 nm is added to limit the saturation of the iCCD camera due to the plasma and to better observe the shock front position at the early delay.

Figure 3 (a) shows selected images of the shock wave propagating in water and following the ablation of an alumina target with a pulse energy of $41 \pm 2 \text{ mJ}$ ($70 \pm 30 \text{ GW/cm}^2$, see supplementary materials). The oblique shock waves correspond to head waves induced by the propagation of leaky Rayleigh surface waves, as well as compression waves propagating in the target close to the interface.

In water, the characteristics of the ablation laser have little importance on shock waves triggering and they have been observed in many configura-

tions [50, 51, 52, 53, 11, 54, 55, 56, 57, 58, 59, 60]. The deposited energy depends on the presence of particles or remaining bubbles from previous pulses [61], which hinders the repeatability of the ablation from pulse to pulse. Moreover, the ablation of particles on the laser path leads to spherical shock waves above the main one [62], complicating the measurement. To limit these phenomena, the water was changed and the cell cleaned every forty laser pulses, corresponding to a full time-shift. Every frame recorded while no ablation sound was heard were discarded. Despite these precautions, the position of the shock wave in water fluctuates much more than in air. At least three reliable repetitions of the measurements were performed for each delay to compute the position of the shock front.

3. Results and discussion

3.1. Propagation in air

The propagation of laser-generated shock waves in air is well described by the similarity model developed by Taylor for the atomic bombs [28, 29]. In particular, the evolution of the position of the shock wave $R(t)$ is given by:

$$R(t) = \left(\frac{E}{\rho_0 K} \right)^{1/5} t^{2/5} \quad (1)$$

with E the energy of the explosion, ρ_0 the density of the air, and K is a dimensionless constant that depends on the heat capacity ratio γ . For a gas composed of diatomic molecules, γ value is 1.4 and K value is 0.856. The maximum pressure at the shock front is then given by:

$$p(R) = 0.155 \frac{E}{R^3} \quad (2)$$

Figure 2 (b) represents the position of the shock wave generated by the ablation of a gold target for 5 different pulse energies (0.09 ± 0.01 , 0.8 ± 0.05 , 2.6 ± 0.2 , 11 ± 1 and 51.6 ± 2 mJ). The position corresponds to the distance perpendicular to the target between the bottom of the plasma and the position of the shock wave. The solid lines correspond to Taylor's model fitted on the experimental data. The effective energy values obtained from the fits are respectively $E = 0.081 \pm 0.04$, 3.73 ± 0.15 , 13.0 ± 0.5 , 43 ± 3 and

110 ± 2 mJ. The model describes very well the experimental data except for the lower pulse energy where the shock wave velocity slows down faster after 100 ns. For such conditions, the overpressure is too low (less than 10 times the atmospheric pressure) and Taylor’s model fails [30]. Excepted for the smallest pulse energy, the energy deduced from the fit using Eq. 1 is systematically over-estimated as reported in previous works [36, 34, 32, 39]. We find that most of the energy contributes to the propagation of the blast wave in the normal direction to the target’s surface. This assumption was introduced by Hall et al. [31] and often mentioned while not investigated [31, 34, 32, 39]. Figure 2 (d) shows the angular distribution of the energy calculated from the position of the shock front according to Taylor’s model (Eq. 1) for a pulse of 7.8 ± 0.2 mJ at $t = 300$ ns. For each angle, the distance of the shock wave is measured from the centre of the ablation spot. In red is represented the angular average of the energy over the hemisphere. The energy appears to be distributed mostly in the direction perpendicular to the target’s surface, explaining the model overestimation of the pulse energy in that direction. The angular average of the energy is very close to the pulse energy as it is a conserved quantity. Previous works already consider such anisotropy [31, 40, 41], but without addressing the angular averaging.

Figure 2 (c) shows the excellent agreement between the energy of the laser pulse and the calculated energy from Taylor’s model averaged on all the emission angles. The model does not depends on the characteristic of the target as shown by measurements on alumina (red dots), paraffin (blue dots) and gold (black dots). It appears that the pulse energy corresponds to the appropriate parameter in the Taylor’s model to reproduce the average shock wave dynamics in air, but the pulse energy does not correspond to the energy stored in the shock wave propagating in air. Indeed, a fraction of the energy is stored in the shock wave propagating in the target and an other fraction corresponds to the plasma formation.

Energies deduced from the fits displayed in figure 2 using Taylor’s model (Eq. 1) are used to compute the pressure as a function of the shock front position according to Eq. 2 (dashed lines in figure 2 (e)). These values are compared to the pressure deduced from the shock front velocity u_s using Rankine-Hugoniot’s relation:

$$p_s(R) = p_\infty \left(1 + \frac{2\gamma}{\gamma + 1} (M_s^2 - 1) \right) \quad (3)$$

with $M_s = u_s/c_0$ the mach number and $c_0 = 340$ m/s the sound velocity

in air. In figure 2 (e), $p_s(R)$ calculated from discrete differential of the position are represented with dots. Solid lines represent the same data using the MATLAB lowess smoothing on positions and velocities to improve the reading.

Taylor’s model and Rankine-Hugoniot’s relation are in good agreement for pressure larger than 1 MPa as expected. For large pressure, Rankine-Hugoniot’s relation converges with Taylor’s model. For lower pressure values, Taylor’s model is no more valid and one should consider other model to describe the shock-front dynamics[30]. At the earliest time, the pressures deduced from the velocity of the shock wave reaches a plateau while Taylor’s model diverges. The initial speed of the shock wave is not as great as expected by Taylor’s model because the energy deposition is never perfectly spatially localised nor instantaneously delivered. We find that Taylor’s model fails to describe the pressure before 20 ns. However, the initial pressure can be easily estimated by Taylor’s model, injecting Eq. 1 in Eq. 2, for an effective time t^* :

$$P(t) = 0.141 \frac{\rho_0^{3/5} E^{2/5}}{t^{*6/5}} \quad (4)$$

with E the pulse energy. In the case of air, $t^* = 10.3$ ns (90% confidence interval [8.4, 13.7]) and $P[\text{MPa}] = (38 \pm 10) \times (E [\text{mJ}])^{2/5}$ at 20 °C (see supplementary information). Despite a focal point of about 100 μm , the pressure remains high even after a few mm which can explain the important damages observed on soft materials like biological tissue in LIBS for instance [63].

3.2. Propagation in water

In the case of propagation in water, the shock front appears mostly hemispherical, with low anisotropy (see figure 3 (a)). We will only discuss the pressure deduced from the velocity of the shock wave in the perpendicular direction to the target’s surface. The shock wave’s velocity can be related to the pressure at the shock front as reported by Vogel et. al [42] using (model 1) the conservation of the momentum at a shock front and the Hugoniot’s curve data determined by Rice and Walsh [43] or (model 2) the Gilmore model and the Tait’s equation of state. In the case of the model 1:

$$p_s = p_\infty + c_1 \rho_0 u_s \left(10^{\frac{u_s - c_0}{c_2}} - 1 \right) \quad (5)$$

with $c_0 = 1483$ m/s the sound velocity in water at 20 °C, $p_\infty = 10^5$ Pa the room pressure, $c_1 = 5190$ m/s, and $c_2 = 25306$ m/s. In the case of the

model 2:

$$p_s = (p_\infty + B) \left(\frac{2nu_s^2}{(n+1)c_0^2} - \frac{n-1}{n+1} \right) - B \quad (6)$$

with $B = 314$ MPa and $n=7$ for water [42] at 20 °C.

Figure 3 (b) represents for 3 different pulse energies (0.8, 2.8 and 27.8 mJ) the position of the shock front. A second-order polynomial curve fit of the shock wave position for $t < 80$ ns (solid lines on figure 3 (b)) provides its initial velocity used for the pressure calculation at the ablation point. When there is no ablation (black dots), a pressure wave traveling at the speed of the sound velocity (red solid line) is still generated because of local heating and fast dilatation of the target's surface. The pressure at the ablation point is reported in figure 3 (c) as a function of the laser intensity [W.cm^{-2}], calculated by dividing the effective pulse energy by its duration and the spot diameter measured on the initial image. Because of non-linearity, some energy is lost in water before reaching the target. We estimated the loss to be 30% and independent of the laser intensity as shown in the supplementary material. The laser intensity reported in figure 3 (c) is an effective laser intensity, accounting for these losses. For the point at the lowest laser intensity, there is no observed plasma. The pressure obtained are consistent with a recent report from Senegacnik et al. [60] for similar experimental conditions (ablation of a target with a nanosecond laser source) and using model 1.

In the case of a confined environment, Fabbro et al. proposed a simple model to determine the pressure at the ablation point depending on the laser intensity [45, 64]:

$$P(\text{MPa}) = 10 \sqrt{\frac{a}{2a+3} ZI} \quad (7)$$

with Z a function of the acoustic impedance such that $2/Z = 1/Z_{\text{water}} + 1/Z_{\text{target}}$, $Z_{\text{water}} = 1.48 \times 10^5 \text{g.cm}^{-2}\text{s}^{-1}$, [65] $Z_{\text{gold}} = 63.6 \times 10^5 \text{g.cm}^{-2}\text{s}^{-1}$, $Z_{\text{alumina}} = 43.3 \times 10^5 \text{g.cm}^{-2}\text{s}^{-1}$, I the laser intensity in GW/cm^2 and a represents the fraction of the pulse energy converted to thermal energy (E_T), keeping in mind that the pressure is defined as $P(t) = \frac{2}{3}E_T(t)$. Z_{gold} and Z_{alumina} are computed from their elastic constants [66].

Figure 3 (c) shows that the pressure follows the square-root dependence on the laser intensity described by Fabbro et al.. The parameter a is fitted on the experimental data (solid lines in figure 3 (c)). The model 2 leads to lower values of the pressure [42] and thus to a lower value of the parameter a :

$a = 0.19$ in the case of model 1 and $a = 0.07$ in the case of model 2. Model 1 uses Hugoniot’s curve data determined by Rice and Walsh [43], valid for large pressures up to 25 GPa. Model 2 uses Tait’s equation of states which fits experimental data for pressure values up to 2.5 GPa [67]. The validity range remains shorter than Rice and Walsh’s data and does not fit fully the pressure range reported in this work. Moreover n and B parameter values can vary of a few percent according to authors [44, 67, 68]. Model 1 appears more reliable. It leads to a value of the parameter a consistent with the ones reported previously for water confinement and nanosecond laser source, from 0.2 to 0.25 [64, 69].

Depending on the model, one can estimate that between 7% and 19% of the pulse energy is converted to thermal energy. In comparison, the dynamics of the bubble generated by the vaporisation of the liquid in similar conditions can be used to estimate the number of vaporised liquid molecules and the corresponding latent heat which represents less than 25% of the pulse [70, 71].

4. Conclusion

In the framework of laser ablation, the dynamics of laser-generated shock waves in air and water is used to determine the pressure at the ablation point. We show that the propagation of laser-generated shock waves in air, following the ablation of a solid target by a nanosecond pulse, is well described by Taylor’s blast auto-similar theory, also named Taylor–von Neumann–Sedov’s blast theory, on a broad range of pulse energy from 0.1 to 50 mJ. However, the shock front is not perfectly hemispherical and goes faster in the direction perpendicular to the target’s surface. It leads to an overestimation of the laser pulse energy using Taylor’s model if looking only at the propagation in the perpendicular direction. However, we show that an angular averaging of the energy distribution leads to a reliable measurement of the pulse energy on the whole range of tested energies and target materials. Comparing the pressure deduced from Taylor’s model to the one deduced from Rankine-Hugoniot’s relation, we show that both are equivalent after 20 ns, but Taylor’s model diverges for shorter delay times while the pressure has reached a plateau. Taylor’s model remains perfectly valid to determine the pressure at the ablation point in air from the laser pulse energy only, keeping its value at $t \simeq 10.3$ ns.

In water, the shock waves velocity is hyper-sonic during the first 50 ns and then reach the sound velocity. The early pressure at the ablation point

is deduced from the initial shock wave velocity. Because of inertial confinement, the pressure is drastically higher than in air and reaches 4 GPa for laser intensity of approximately 70 GW/cm². We show that the initial pressure deduced from the shock waves increases as the square root of the laser intensity, following the analytical model developed by Fabbro and co-workers, on a broad range of laser intensity, and on both gold and alumina targets. One can thus use this simple model considering only the acoustic impedance of the target and liquid, and the laser intensity in order to determine the pressure at the ablation point.

CRedit authorship contribution statement

Arsène Chemin: Conceptualization, Methodology, Investigation, Validation, Formal analysis, Writing - Original Draft, Visualization. **Mehdi W. Fawaz:** Investigation, Validation, Formal analysis. **David Amans:** Conceptualization, Writing - Original Draft, Supervision, Project administration.

Declaration of Competing Interest

The authors declare that they have no known competing financial interests or personal relationships that could have appeared to influence the work reported in this paper.

References

- [1] A. Vogel, V. Venugopalan, Mechanisms of pulsed laser ablation of biological tissues, *Chem. Rev.* 103 (2003) 577–644. doi:10.1021/cr010379n.
- [2] H. K. Nguendon, N. Faivre, B. Meylan, S. Shevchik, G. Rauter, R. Guzman, P. C. Cattin, K. Wasmer, A. Zam, Characterization of ablated porcine bone and muscle using laser-induced acoustic wave method for

- tissue differentiation, in: European Conference on Biomedical Optics, Optical Society of America, 2017, p. 104170N. doi:10.1117/12.2286121.
- [3] Z. Chen, A. Bogaerts, A. Vertes, Phase explosion in atmospheric pressure infrared laser ablation from water-rich targets, *Appl. Phys. Lett.* 89 (2006) 041503. doi:10.1063/1.2243961.
- [4] S. Lee, T. Anderson, H. Zhang, T. J. Flotte, A. G. Doukas, Alteration of cell membrane by stress waves in vitro, *Ultrasound Med. Biol.* 22 (1996) 1285–1293. doi:10.1016/S0301-5629(96)00149-4.
- [5] S. Kraft, J. Schille, S. Mauersberger, L. Schneider, U. Loeschner, Pump-probe imaging for process control and optimization in high-speed laser micro machining, in: *Laser-based Micro-and Nanoprocessing XIV*, volume 11268, International Society for Optics and Photonics, 2020, p. 112681H. doi:10.1117/12.2545021.
- [6] J. Metelkova, D. Ordnung, Y. Kinds, B. Van Hooreweder, Novel strategy for quality improvement of up-facing inclined surfaces of LPBF parts by combining laser-induced shock waves and in situ laser remelting, *J. Mater. Process. Technol.* 290 (2021) 116981. doi:10.1016/j.jmatprotec.2020.116981.
- [7] A. Al-Kattan, D. Grojo, C. Drouet, A. Mouskeftaras, P. Delaporte, A. Casanova, J. D. Robin, F. Magdinier, P. Alloncle, C. Constantinescu, V. Motto-Ros, J. Hermann, Short-Pulse Lasers: A Versatile Tool in Creating Novel Nano-/Micro-Structures and Compositional Analysis for Healthcare and Wellbeing Challenges, *Nanomaterials* 11 (2021) 712. doi:10.3390/nano11030712.
- [8] K. Manes, M. Spaeth, J. Adams, M. Bowers, J. Bude, C. Carr, A. Conder, D. Cross, S. Demos, J. D. Nicola, et al., Damage mechanisms avoided or managed for NIF large optics, *Fusion Sci. Technol.* 69 (2016) 146–249. doi:10.13182/FST15-139.
- [9] X. Zhang, Y. Jiang, R. Qiu, J. Meng, J. Cao, C. Zhang, Y. Zhao, T. Lü, Concentric ring damage on the front surface of fused silica induced by a nanosecond laser, *Opt. Mater. Express* 9 (2019) 4811–4817. doi:10.1364/OME.9.004811.

- [10] D. Kraus, A. Ravasio, M. Gauthier, D. O. Gericke, J. Vorberger, S. Frydrych, J. Helfrich, L. B. Fletcher, G. Schaumann, B. Nagler, B. Barbrel, B. Bachmann, E. J. Gamboa, S. Goede, E. Granados, G. Gregori, H. J. Lee, P. Neumayer, W. Schumaker, T. Doeppner, R. W. Falcone, S. H. Glenzer, M. Roth, Nanosecond formation of diamond and lonsdaleite by shock compression of graphite, *Nat. Commun.* 7 (2016) 10970. doi:10.1038/ncomms10970.
- [11] D. Amans, M. Diouf, J. Lam, G. Ledoux, C. Dujardin, Origin of the nano-carbon allotropes in pulsed laser ablation in liquids synthesis, *J. Colloid Interface Sci.* 489 (2017) 114–125. doi:10.1016/j.jcis.2016.08.017.
- [12] X. D. Ren, S. X. Tang, L. M. Zheng, S. Q. Yuan, N. F. Ren, H. M. Yang, Y. Wang, W. F. Zhou, S. D. Xu, Direct transfer-adsorption: The new molecular dynamics transition mechanism of nano-diamond preparation by laser shock processing, *J. Cryst. Growth* 421 (2015) 1–7. doi:10.1016/j.jcrysgro.2015.03.050.
- [13] B. Chide, S. Maurice, A. Cousin, B. Bousquet, D. Mimoun, O. Beyssac, P.-Y. Meslin, R. C. Wiens, Recording laser-induced sparks on mars with the supercam microphone, *Spectroc. Acta B* 174 (2020) 106000. doi:10.1016/j.sab.2020.106000.
- [14] Q. Ma, V. Motto-Ros, X. Bai, J. Yu, Experimental investigation of the structure and the dynamics of nanosecond laser-induced plasma in 1-atm argon ambient gas, *Appl. Phys. Lett.* 103 (2013) 204101. doi:10.1063/1.4829628.
- [15] B. Pokrzywka, A. Mendys, K. Dzierżega, M. Grabiec, S. Pellerin, Laser light scattering in a laser-induced argon plasma: Investigations of the shock wave, *Spectroc. Acta B* 74 (2012) 24–30. doi:10.1016/j.sab.2012.06.015.
- [16] D. M. Surmick, D. J. Dagel, C. G. Parigger, Spatial molecular AIO temperature distributions in laser-induced plasma, *Atoms* 7 (2019) 86. doi:10.3390/atoms7030086.
- [17] T. Itina, A. Voloshko, Nanoparticle formation by laser ablation in air and by spark discharges at atmospheric pressure, *Appl. Phys. B* 113 (2013) 473–478. doi:10.1007/s00340-013-5490-6.

- [18] D. Amans, W. Cai, S. Barcikowski, Status and demand of research to bring laser generation of nanoparticles in liquids to maturity, *Appl. Surf. Sci.* 488 (2019) 445–454. doi:10.1016/j.apsusc.2019.05.117.
- [19] V. Amendola, D. Amans, Y. Ishikawa, N. Koshizaki, S. Scire, G. Compagnini, S. Reichenberger, S. Barcikowski, Room-Temperature Laser Synthesis in Liquid of Oxide, Metal-Oxide Core-Shells, and Doped Oxide Nanoparticles, *Chem.-Eur. J.* 26 (2020) 9206–9242. doi:10.1002/chem.202000686.
- [20] E. Fazio, B. Goekce, A. De Giacomo, M. Meneghetti, G. Compagnini, M. Tommasini, F. Waag, A. Lucotti, C. G. Zanchi, P. M. Ossi, M. Dell’Aglia, L. D’Urso, M. Condorelli, V. Scardaci, F. Biscaglia, L. Litti, M. Gobbo, G. Gallo, M. Santoro, S. Trusso, F. Neri, Nanoparticles Engineering by Pulsed Laser Ablation in Liquids: Concepts and Applications, *Nanomaterials* 10 (2020) 2317. doi:10.3390/nano10112317.
- [21] R. C. Forsythe, C. P. Cox, M. K. Wilsey, A. M. Müller, Pulsed laser in liquids made nanomaterials for catalysis, *Chem. Rev.* 121 (2021) 7568–7637. doi:10.1021/acs.chemrev.0c01069.
- [22] S. Reichenberger, G. Marzun, M. Muhler, S. Barcikowski, Perspective of Surfactant-free Colloidal Nanoparticles in Heterogeneous Catalysis, *ChemCatChem* 11 (2019) 4489–4518. doi:10.1002/cctc.201900666.
- [23] H. Du, V. Castaing, D. Guo, B. Viana, Rare-earths doped-nanoparticles prepared by pulsed laser ablation in liquids, *Ceram. Int.* 46 (2020) 26299–26308. doi:10.1016/j.ceramint.2020.04.291.
- [24] S.-X. Liang, L.-C. Zhang, S. Reichenberger, S. Barcikowski, Design and perspective of amorphous metal nanoparticles from laser synthesis and processing, *Phys. Chem. Chem. Phys.* 23 (2021) 11121–11154. doi:10.1039/D1CP00701G.
- [25] A. Kanitz, M.-R. Kalus, E. L. Gurevich, A. Ostendorf, S. Barcikowski, D. Amans, Review on experimental and theoretical investigations of the early stage, femtoseconds to microseconds processes during laser ablation in liquid-phase for the synthesis of colloidal nanoparticles, *Plasma Sources Sci. Technol.* 28 (2019) 103001. doi:10.1088/1361-6595/ab3dbe.

- [26] S. Barcikowski, A. Plech, K. S. Suslick, A. Vogel, Materials synthesis in a bubble, *MRS Bull.* 44 (2019) 382–391. doi:10.1557/mrs.2019.107.
- [27] J. Lam, V. Motto-Ros, D. Misiak, C. Dujardin, G. Ledoux, D. Amans, Investigation of local thermodynamic equilibrium in laser-induced plasmas: Measurements of rotational and excitation temperatures at long time scales, *Spectroc. Acta Pt. B-Atom. Spectr.* 101 (2014) 86–92. doi:10.1016/j.sab.2014.07.013.
- [28] G. I. Taylor, The formation of a blast wave by a very intense explosion. I. theoretical discussion, *Proc. R. Soc. Lond. A* 201 (1950) 159–174. doi:10.1098/rspa.1950.0049.
- [29] G. I. Taylor, The formation of a blast wave by a very intense explosion. II. the atomic explosion of 1945, *Proc. R. Soc. Lond. A* 201 (1950) 175–186. doi:10.1098/rspa.1950.0050.
- [30] D. L. Jones, Intermediate strength blast wave, *Phys. Fluids* 11 (1968) 1664. doi:10.1063/1.1692177.
- [31] R. B. Hall, Laser production of blast waves in low pressure gases, *Journal of Applied Physics* 40 (1969) 1941–1945. doi:10.1063/1.1657871.
- [32] C. Porneala, D. A. Willis, Time-resolved dynamics of nanosecond laser-induced phase explosion, *J. Phys. D* 42 (2009) 155503. doi:10.1088/0022-3727/42/15/155503.
- [33] S. Palanco, S. Marino, M. Gabás, S. Bijani, L. Ayala, J. R. Ramos-Barrado, Particle formation and plasma radiative losses during laser ablation suitability of the sedov-taylor scaling, *Opt. Express* 22 (2014) 16552–16557. doi:10.1364/OE.22.016552.
- [34] S. H. Jeong, R. Greif, R. E. Russo, Shock wave and material vapour plume propagation during excimer laser ablation of aluminium samples, *J. Phys. D* 32 (1999) 2578. doi:10.1088/0022-3727/32/19/316/meta.
- [35] T. A. Schmitz, J. Koch, D. Guenther, R. Zenobi, Early plume and shock wave dynamics in atmospheric-pressure ultraviolet-laser ablation of different matrix-assisted laser ablation matrices, *J. Appl. Phys.* 109 (2011) 123106. doi:10.1063/1.3592651.

- [36] S. Jeong, R. Greif, R. Russo, Propagation of the shock wave generated from excimer laser heating of aluminum targets in comparison with ideal blast wave theory, *Appl. Surf. Sci.* 127 (1998) 1029–1034. doi:10.1016/S0169-4332(97)00785-X.
- [37] X. Chen, B. M. Bian, Z. H. Shen, J. Lu, X. W. Ni, Equations of laser-induced plasma shock wave motion in air, *Microw. Opt. Technol. Lett.* 38 (2003) 75–79. doi:10.1002/mop.10975.
- [38] Z. Chen, A. Vertes, Early plume expansion in atmospheric pressure midinfrared laser ablation of water-rich targets, *Phys. Rev. E* 77 (2008) 036316. doi:10.1103/PhysRevE.77.036316.
- [39] J. Diaci, J. Možina, A study of blast waveforms detected simultaneously by a microphone and a laser probe during laser ablation, *Appl. Phys. A* 55 (1992) 352–358. doi:10.1007/BF00324084.
- [40] J. J. Yoh, H. Lee, J. Choi, K.-c. Lee, K.-h. Kim, Ablation-induced explosion of metal using a high-power Nd:YAG laser, *J. Appl. Phys.* 103 (2008) 043511. doi:10.1063/1.2884532.
- [41] C. Phelps, C. J. Druffner, G. P. Perram, R. R. Biggers, Shock front dynamics in the pulsed laser deposition of $\text{YBa}_2\text{Cu}_3\text{O}_{7-x}$, *J. Phys. D* 40 (2007) 4447. doi:10.1088/0022-3727/40/15/010/meta.
- [42] A. Vogel, S. Busch, U. Parlitz, Shock wave emission and cavitation bubble generation by picosecond and nanosecond optical breakdown in water, *J. Acoust. Soc. Am.* 100 (1996) 148–165. doi:10.1121/1.415878.
- [43] M. H. Rice, J. M. Walsh, Equation of state of water to 250 kilobars, *The Journal of Chemical Physics* 26 (1957) 824–830. doi:10.1063/1.1743415.
- [44] J. M. Richardson, A. B. Arons, R. R. Halverson, Hydrodynamic properties of sea water at the front of a shock wave, *J. Chem. Phys.* 15 (1947) 785–794. doi:10.1063/1.1746334.
- [45] R. Fabbro, J. Fournier, P. Ballard, D. Devaux, J. Virmont, Physical study of laser-produced plasma in confined geometry, *J. Appl. Phys.* 68 (1990) 775–784. doi:10.1063/1.346783.

- [46] H. Li, E. A. Ghezal, A. Nehari, G. Alombert-Goget, A. Brenier, K. Lebbou, Bubbles defects distribution in sapphire bulk crystals grown by Czochralski technique, *Opt. Mater.* 35 (2013) 1071. doi:10.1016/j.optmat.2012.12.022.
- [47] H. Li, E. A. Ghezal, G. Alombert-Goget, G. Breton, J. M. In-gargiola, A. Brenier, K. Lebbou, Qualitative and quantitative bubbles defects analysis in undoped and Ti-doped sapphire crystals grown by Czochralski technique, *Opt. Mater.* 37 (2014) 132. doi:10.1016/j.optmat.2014.05.012.
- [48] P. Gregorcic, J. Mozina, High-speed two-frame shadowgraphy for velocity measurements of laser-induced plasma and shock-wave evolution, *Opt. Lett.* 36 (2011) 2782–2784. doi:10.1364/OL.36.002782.
- [49] P. Gregorcic, J. Diaci, J. Mozina, Two-dimensional measurements of laser-induced breakdown in air by high-speed two-frame shadowgraphy, *Appl. Phys. A-Mater. Sci. Process.* 112 (2013) 49–55. doi:10.1007/s00339-012-7173-2.
- [50] K. Sasaki, T. Nakano, W. Soliman, N. Takada, Effect of pressurization on the dynamics of a cavitation bubble induced by liquid-phase laser ablation, *Appl. Phys. Express* 2 (2009) 046501. doi:10.1143/apex.2.046501.
- [51] M. Tiberi, A. Simonelli, G. Cristoforetti, P. Marsili, F. Giammanco, E. Giorgetti, Effect of picosecond laser induced cavitation bubbles generated on Au targets in a nanoparticle production set-up, *Appl. Phys. A-Mater. Sci. Process.* 110 (2013) 857–861. doi:10.1007/s00339-012-7165-2.
- [52] J. Tomko, J. J. Naddeo, R. Jimenez, Y. Tan, M. Steiner, J. M. Fitz-Gerald, D. M. Bubb, S. M. O’Malley, Size and polydispersity trends found in gold nanoparticles synthesized by laser ablation in liquids, *Phys. Chem. Chem. Phys.* 17 (2015) 16327–16333. doi:10.1039/c5cp01965f.
- [53] R. Tanabe, T. T. P. Nguyen, T. Sugiura, Y. Ito, Bubble dynamics in metal nanoparticle formation by laser ablation in liquid studied through high-speed laser stroboscopic videography, *Appl. Surf. Sci.* 351 (2015) 327–331. doi:10.1016/j.apsusc.2015.05.030.

- [54] T. T. P. Nguyen, R. Tanabe, Y. Ito, Comparative study of the expansion dynamics of laser-driven plasma and shock wave in in-air and underwater ablation regimes, *Opt. Laser Technol.* 100 (2018) 21–26. doi:10.1016/j.optlastec.2017.09.021.
- [55] T. T. P. Nguyen, R. Tanabe-Yamagishi, Y. Ito, Effects of liquid depth on the expansion and collapse of a hemispherical cavitation bubble induced in nanosecond pulsed laser ablation of a solid in liquid, *Opt. Lasers Eng.* 126 (2020) 105937. doi:10.1016/j.optlaseng.2019.105937.
- [56] J. Long, M. Eliceiri, Z. Vangelatos, Y. Rho, L. Wang, Z. Su, X. Xie, Y. Zhang, C. P. Grigoropoulos, Early dynamics of cavitation bubbles generated during ns laser ablation of submerged targets, *Opt. Express* 28 (2020) 14300–14309. doi:10.1364/OE.391584.
- [57] L. Marti-Lopez, R. Ocana, J. A. Porro, M. Morales, J. L. Ocana, Optical observation of shock waves and cavitation bubbles in high intensity laser-induced shock processes, *Appl. Optics* 48 (2009) 3671–3680. doi:10.1364/AO.48.003671.
- [58] H. Hu, T. Liu, H. Zhai, Comparison of femtosecond laser ablation of aluminum in water and in air by time-resolved optical diagnosis, *Opt. Express* 23 (2015) 628–635. doi:10.1364/OE.23.000628.
- [59] Z. Zhang, A. Wang, J. Wu, Y. Liu, D. Huang, Y. Qiu, J. Li, Spatial confinement effects of bubbles produced by laser ablation in liquids, *AIP Adv.* 9 (2019) 125048. doi:10.1063/1.5127261.
- [60] M. Senegacnik, K. Kunimoto, S. Yamaguchi, K. Kimura, T. Sakka, P. Gregorcic, Dynamics of laser-induced cavitation bubble during expansion over sharp-edge geometry submerged in liquid - an inside view by diffuse illumination, *Ultrason. Sonochem.* 73 (2021) 105460. doi:10.1016/j.ultsonch.2021.105460.
- [61] S. Dittrich, S. Barcikowski, B. Goekce, Plasma and nanoparticle shielding during pulsed laser ablation in liquids cause ablation efficiency decrease, *Opto-Electron. Adv.* 4 (2021) 200072. doi:10.29026/oea.2021.200072.

- [62] I. V. Baimler, A. V. Simakin, V. K. Chevokin, V. A. Podvyaznikov, S. V. Gudkov, Features of optical breakdown of aqueous colloidal solutions of ferric oxide (Fe_2O_3) nanoparticles occurring on individual or on two closely located nanoparticles, *Chemical Physics Letters* 776 (2021) 138697. doi:10.1016/j.cplett.2021.138697.
- [63] Y. Gimenez, B. Busser, F. Trichard, A. Kulesza, J. M. Laurent, V. Zaun, F. Lux, J. M. Benoit, G. Panczer, P. Dugourd, O. Tillement, F. Pelascini, L. Sancey, V. Motto-Ros, 3D Imaging of Nanoparticle Distribution in Biological Tissue by Laser-Induced Breakdown Spectroscopy, *Sci Rep* 6 (2016) 29936. doi:10.1038/srep29936.
- [64] L. Berthe, R. Fabbro, P. Peyre, L. Tollier, E. Bartnicki, Shock waves from a water-confined laser-generated plasma, *J. Appl. Phys.* 82 (1997) 2826–2832. doi:10.1063/1.366113.
- [65] D. L. Bradley, W. D. Wilson, Acoustic impedance of sea water as a function of temperature, pressure and salinity, volume NOLTR 66-146, U.S. Naval Ordnance Laboratory, White Oak, Maryland, 1966.
- [66] H. P. R. Frederikse, Elastic constants of single crystals, in: J. R. Rumble (Ed.), *CRC Handbook of Chemistry and Physics*, 101 ed., CRC Press/Taylor & Francis, Boca Raton, FL., 2020.
- [67] S. Ridah, Shock waves in water, *J. Appl. Phys.* 64 (1988) 152–158. doi:10.1063/1.341448.
- [68] Y. H. LI, Equation of state of water and sea water, *J. Geophys. Res.* 72 (1967) 2665. doi:10.1029/JZ072i010p02665.
- [69] D. Devaux, R. Fabbro, L. Tollier, E. Bartnicki, Generation of shock-waves by laser-induced plasma in confined geometry, *J. Appl. Phys.* 74 (1993) 2268–2273. doi:10.1063/1.354710.
- [70] J. Lam, J. Lombard, C. Dujardin, G. Ledoux, S. Merabia, D. Amans, Dynamical study of bubble expansion following laser ablation in liquids, *Applied Physics Letters* 108 (2016) 074104. doi:10.1063/1.4942389.
- [71] A. Chemin, J. Lam, G. Laurens, F. Trichard, V. Motto-Ros, G. Ledoux, V. Jary, V. Laguta, M. Nikl, C. Dujardin, D. Amans, Doping nanoparticles using pulsed laser ablation in a liquid containing the doping agent, *Nanoscale Adv.* 1 (2019) 3963–3972. doi:10.1039/c9na00223e.

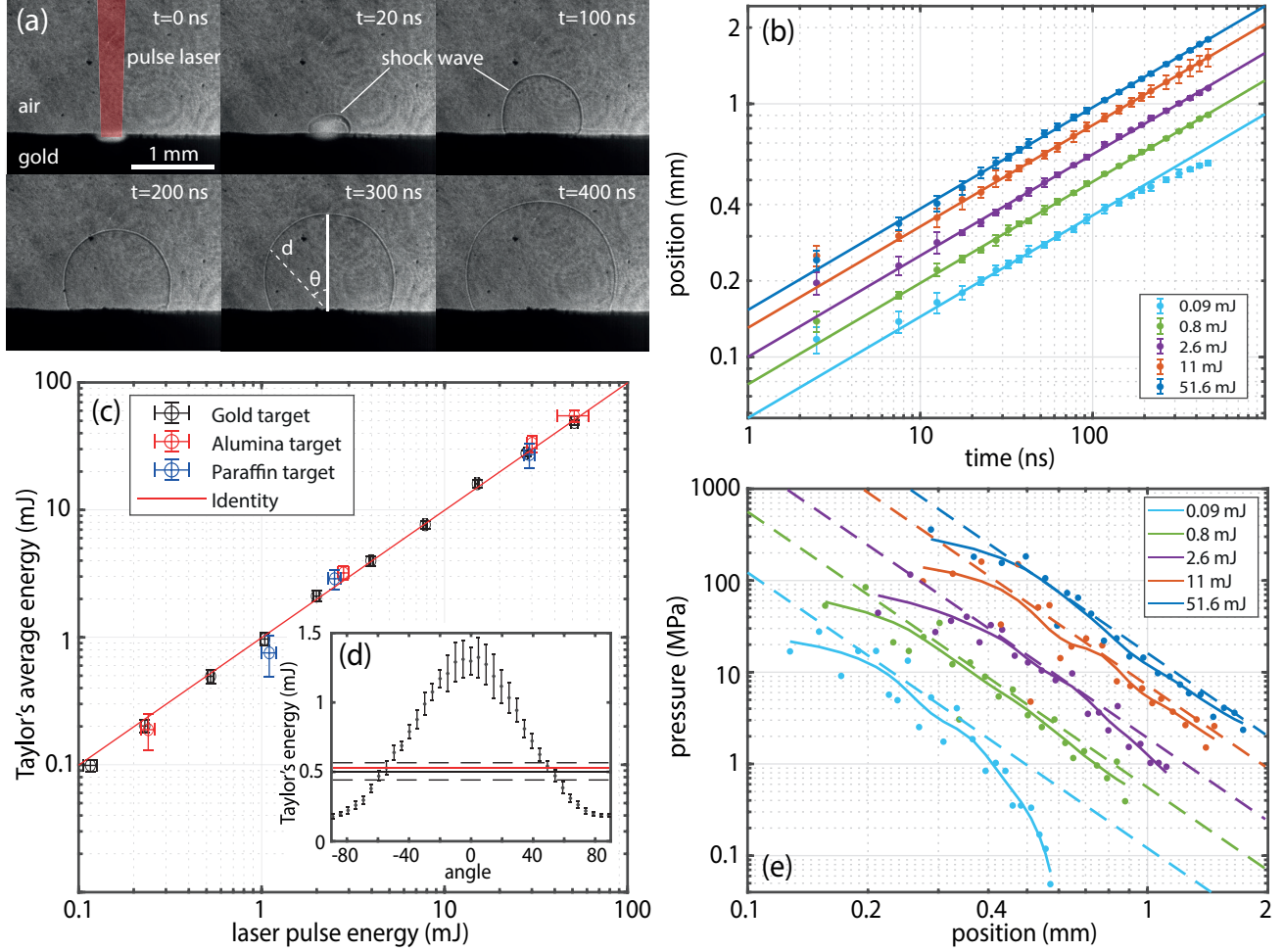


Figure 2: (a) Shadographs of the ablation in air of a gold target for different delay times. (b) Time evolution of the shock front position. Black line corresponds to Taylor's model with a time dependence $t^{\frac{2}{5}}$. (c) Comparison between the energy obtained from Taylor's model averaged in every direction and the measured energy of the laser pulse. Red line corresponds to the identity function. (d) Energy determined from the shock wave's position for a 300 ns delay according to Taylor's model for different angles. The pulse energy is 0.53 ± 0.02 mJ. The Black line corresponds to the angular average (see supplementary information) and the red line is the measured pulse energy. (e) Pressure of the shock wave determined from the shock front's velocity using Rankine-Hugoniot's relation (Eq. 3). Dots correspond to discrete differential, solid lines are pressures calculated from smooth data as eye guideline and solid dashed line corresponds to Taylor's model (Eq. 2) with the energies fitted on the position in panel (b) and using Eq. 1.

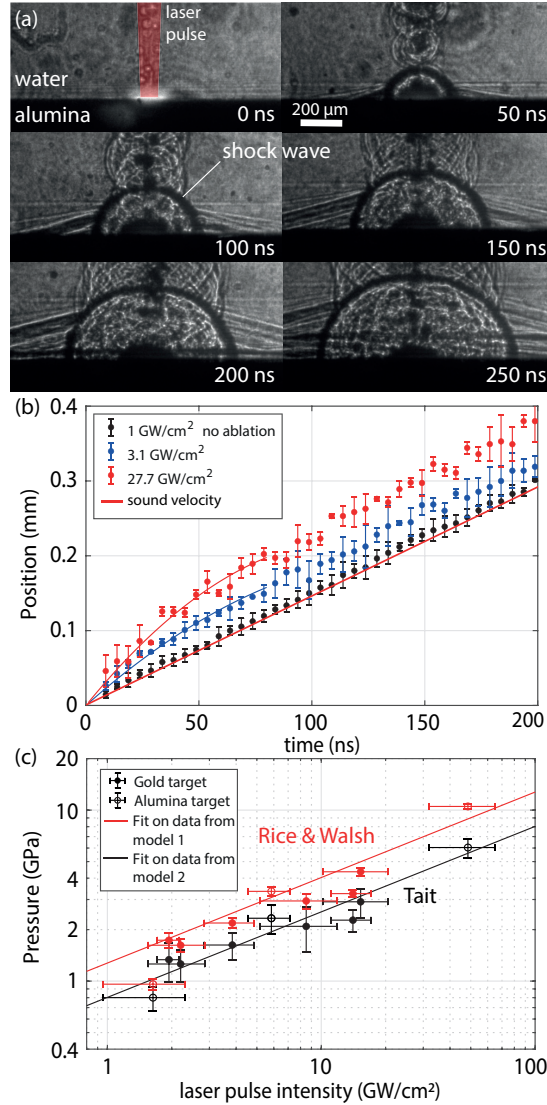
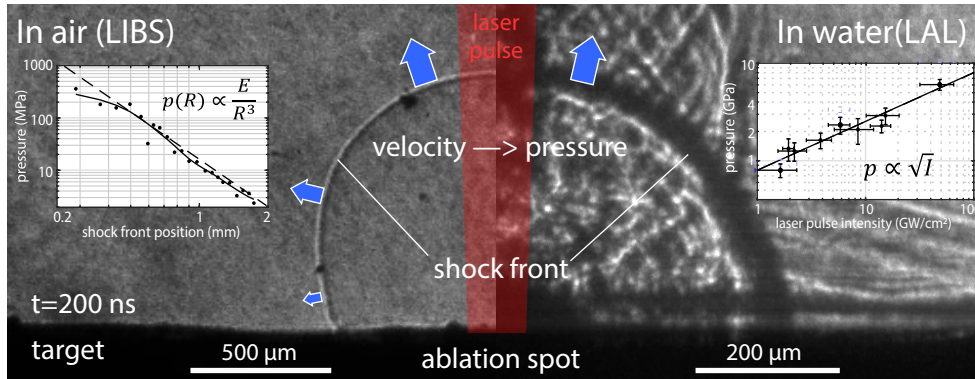


Figure 3: (a) Shadowgraphs of the ablation of an alumina target underwater. (b) Positions of the shock front following the laser ablation of a gold target at various laser intensities. The straight red line corresponds to a propagation at the sound velocity (1483 m/s). The deceleration observed in the early 60 ns is fitted by a second-order polynomial curve (solid lines). (c) Evolution of the pressure depending on the laser intensity for gold target (solid dots) and alumina target (circles) using Eq. 5 (model 1, red) and Eq. 6 (model 2, black). The solid lines correspond to the fits using Eq. 7 from Fabbro et al. [45] and leading to $a = 0.19$ and $a = 0.07$, respectively.

Graphical Abstract

Investigation of the blast pressure following laser ablation at a solid-fluid interface using shock waves dynamics in air and in water

Arsène Chemin, Mehdi W. Fawaz, David Amans



Highlights

Investigation of the blast pressure following laser ablation at a solid-fluid interface using shock waves dynamics in air and in water

Arsène Chemin, Mehdi W. Fawaz, David Amans

- The pressure is determined from shock waves dynamics for ablation in air and water.
- The anisotropy in the Taylor–von Neumann–Sedov blast wave is characterized.
- In air, the initial pressure is defined by the pulse energy.
- In liquids, the initial pressure follows the square root of the laser intensity.
- In liquids, 19% of the energy of a nanosecond pulse lead to thermal energy.